High-accuracy microwave and optical frequency standards using laser-cooled Hg^+ ions

D.J. Berkeland, J.D. Miller, F.C. Cruz, B.C. Young, J.C. Bergquist, W.M. Itano, and D.J. Wineland
National Institute of Standards and Technology, Time and Frequency Division
Boulder, CO 80303

We discuss frequency standards based on laser-cooled $^{199}Hg^+$ ions confined in cryogenic rf (Paul) traps. In one experiment, the frequency of a microwave source is servoed to the ions' ground-state hyperfine transition at 40.5 GHz. For seven ions and a Ramsey free precession time of 100 s, the fractional frequency stability is $3.3\,(2) \times 10^{-13}\,\tau^{-1/2}$ for measurement times $\tau < 2$ h. The ground-state hyperfine interval is measured to be 40 507 347 996.841 59 (20) (41) Hz, where the first number in parentheses is the uncertainty due to statistics and systematic effects, and the second is the uncertainty in the frequency of the time scale to which the standard is compared. In a second experiment under development, a strong-binding cryogenic trap will confine a single ion used for an optical frequency standard based on a narrow electric quadrupole transition at 282 nm. The bandwidth of the laser used to drive this transition is less than 10 Hz at 563 nm.

Introduction

Trapped and cooled ions are useful in atomic physics for several reasons. The ions can be benignly held in a well-controlled environment, significantly reducing systematic effects such as Stark and Zeeman shifts. The same ions can be observed repeatedly and for very long times, so that narrow atomic transitions can be observed with extremely high resolution. Finally, it is possible to observe and manipulate the quantum states of individual ions, leading to measurements of quantum mechanical effects such as quantum jumps [1] and the preparation of the atoms' internal states toward, for example, spin squeezing [2]. For all of these reasons, trapped and cooled ions are particularly well suited for time and frequency standards. Stable and accurate atomic frequency standards [3] are not only useful for measuring time, but often are the realization of other basic units, are necessary in navigation and communication, and frequently are used in investigations of physical phenomena [4].

Groups at NASA's Jet Propulsion Laboratory (JPL) and Australia's Commonwealth Scientific and Industrial Research Organisation (CSIRO) have demonstrated highly stable clocks that use linear rf (Paul) traps to store buffer-gas-cooled ions [5, 6]. In these traps, most of the ions lie away from the nodal line of the trap's rf electric field. For these ions, the atomic motion driven by the oscillating trap field (micromotion) induces significant second-order Doppler (time-dilation) shifts of the average atomic transition frequency. At NIST, our goal is to develop frequency standards that achieve high accuracy in addition to high stability. We confine strings of laser-cooled $^{199}Hg^+$ ions in a linear rf trap such as that depicted in Fig. 1 [7]. A linear trap can confine many laser-cooled ions along the rf nodal line, where Doppler shifts and ac Stark shifts are minimum [8, 9]. Furthermore, if all the ions crystallize along the rf nodal line, there is minimal heating from the trapping fields. Thus, perturbative cooling laser radiation can be removed during the long probe periods of the clock transition. We use $^{199}Hg^+$, which offers a microwave clock transition at 40.5 GHz and an optical clock transition at 1.06×10^{15} Hz (see Fig. 2). To first-order, both transitions are insensitive to magnetic and electric fields at zero fields. Using linear crystals of $^{199}Hg^+$ ions, we expect to reduce all systematic shifts to less than a part in 10^{16}.

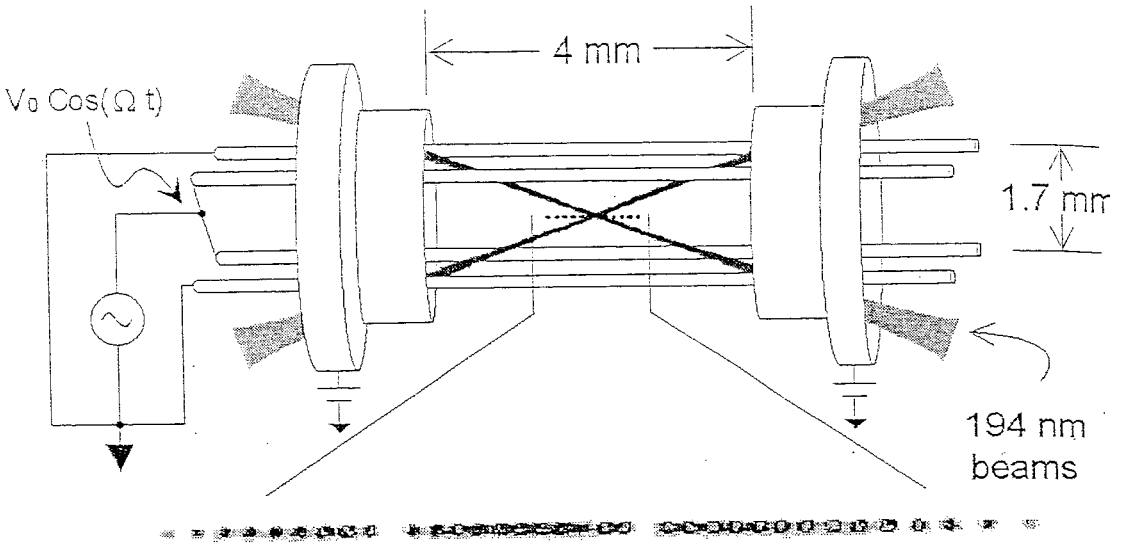

Figure 1: Linear rf trap, and an image of a string of ions. The ions are spaced approximately 10 μm apart, and apparent gaps in the ion string are due to ions other than $^{199}Hg^+$, which do not fluoresce at the frequencies of the 194 nm laser beams. The spatial extent of the ions is exaggerated for clarity; in reality the laser beams overlap all the ions.

If the fluctuations of the atomic signal are due only to quantum statistics, then the stability of a frequency source servoed to the atomic transition is given by [10, 11]

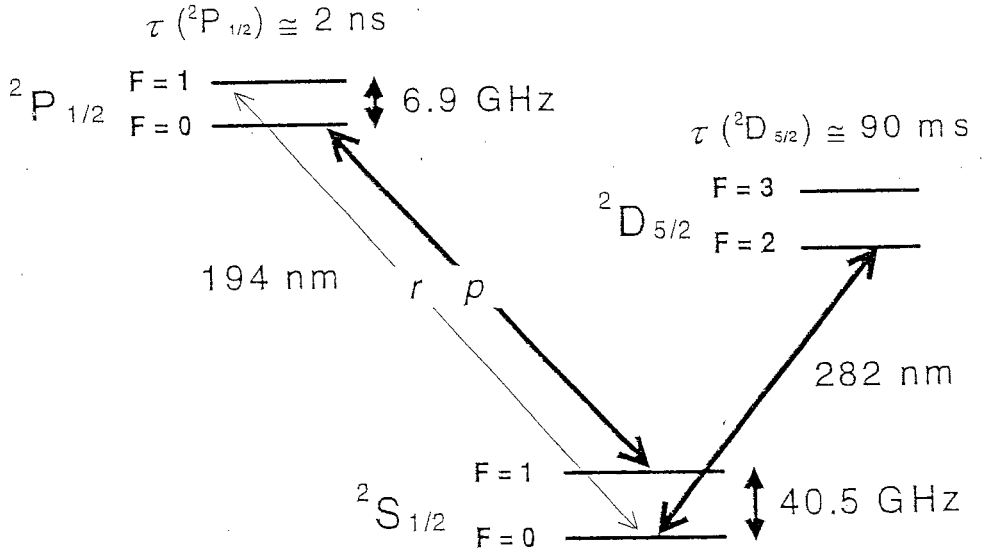

Figure 2: Partial energy diagram of $^{199}Hg^+$. The 70 MHz wide 194 nm transitions are used for laser cooling and detection. The 40.5 GHz and 282 nm transitions are the clock transitions.

$$\sigma_y(\tau) = \frac{1}{\omega_0 \sqrt{N\, T_R}}\, \tau^{-1/2}, \qquad (1)$$

where ω_0 is the frequency of the atomic transition, N is the number of ions, T_R is the Ramsey interrogation time, and τ is the averaging time of the measurement. For the ground-state hyperfine transition, $\omega_0/2\pi = 40.5$ GHz. It appears feasible to use $N = 100$ ions and $T_R = 100$ s, which gives $\sigma_y(\tau) \approx 4 \times 10^{-14}\, \tau^{-1/2}$. For the 282 nm $5d^{10}6s\ ^2S_{1/2} \rightarrow 5d^9 6s^2\ ^2D_{5/2}$ electric quadrupole transition, $\omega_0/2\pi = 10^{15}$ Hz, so that using $N = 1$ and $T_R =$ 25 ms gives $\sigma_y(\tau) = 10^{-15}\, \tau^{-1/2}$.

We report a preliminary evaluation of a clock based on the 40.5 GHz ground-state hyperfine transition in $^{199}Hg^+$. We also discuss the development of a frequency standard based on the 282 nm electric quadrupole transition, and the narrow band source of 563 nm radiation needed to drive this transition. We describe the laser systems for these experiments and the progress toward more compact solid-state systems.

Cryogenic Linear rf Trap

Figure 1 shows the linear rf trap used in the 40.5 GHz microwave clock. Two diagonally opposite rods are held at static and rf potential ground. The potential of the other two rods is $V_0 \cos(\Omega t)$, where $V_0 \approx 150$ V and $\Omega/2\pi = 8.6$ MHz. The resulting pseudopotential confines the ions radially in a well with a secular frequency $\omega_r/2\pi \approx 230$ kHz. Insulated wires are threaded through the rods to heat them, which removes patch fields and electrical charge that otherwise leave the electrodes only slowly in the cryogenic environment. To confine the ions axially, two cylindrical sections at either end of the trap are held at a potential of approximately +10 V. The resulting axial potential well has a secular frequency of $\omega_z/2\pi \approx 15$ kHz. The ions are laser-cooled using the 194 nm, $5d^{10}6s\ ^2S_{1/2} \rightarrow 5d^{10}6p\ ^2P_{1/2}$ electric dipole transitions shown in Fig. 2. Typically, a string of approximately ten ions is confined along the trap axis. By minimizing the ion micromotion in all three dimensions, we assure that the laser-cooled ions lie along the rf nodal line [12].

We place the trap in a cryogenic environment to reduce problems associated with background gas. Previously, we used a linear rf trap at room temperature with a background pressure of approximately 10^{-8} Pa [13]. At this pressure, background neutral Hg atoms cause Hg^+ loss, presumably by forming dimers with ions excited by the cooling laser. The resulting lifetime of ions in the trap was about ten minutes. At liquid He temperatures, however, Hg and most other background gases are cryopumped onto the walls of the chamber. In this low-pressure environment, we have trapped Hg^+ ions in the presence of laser radiation without loss for periods of over ten hours. Even in the absence of laser cooling during overnight down periods, we have confined strings of approximately ten ions for several days. With this low background pressure, most pressure shifts should be negligible, although, since helium is not efficiently cryopumped, it may cause a pressure shift.

Operation at 4 K also reduces the frequency shifts due to blackbody radiation. For the ground-state hyperfine transition, at $T = 4$ K, the fractional blackbody Zeeman shift is -2×10^{-21}, and the fractional blackbody Stark shift is -3×10^{-24} [14]. This is significantly smaller than the fractional blackbody Stark shift for neutral cesium $(1.69(4) \times 10^{-14}$ at $T = 300$ K [14]).

Laser-atom Interactions

Laser beams at 194 nm are used for both cooling and state detection. For cooling, transition p is used because it is the closest to a cycling transition (see Fig. 2). The frequency

of the primary laser is tuned slightly below resonance with this transition, but can off-resonantly excite the ion into the $^2P_{1/2}$, $F = 1$ level, from which the ion can decay into the $^2S_{1/2}$, $F = 0$ level. To maintain fluorescence, a repumping laser beam, resonant with transition r, is overlapped collinearly with the primary laser beam.

To determine the atomic state, the primary beam is pulsed on for a time comparable to the time necessary to pump the ions from the $^2S_{1/2}$, $F = 1$ to the $^2S_{1/2}$, $F = 0$ level (typically 10 ms). If the ion is found in the $^2S_{1/2}$, $F = 1$ level, it will scatter about 10^4 photons before it optically pumps into the $^2S_{1/2}$, $F = 0$ level. We detect and count approximately 150 of these photons. If the transition is not saturated, the number of photons scattered before the ion is optically pumped can be made nearly insensitive to laser power. Thus the signal-to-noise ratio of the state detection signal can be limited only by quantum projection noise [15] if the ions are monitored individually. Currently, however, the state-detection signal is simply the combined fluorescence from all the ions. As a result, we think that fluctuations in the frequency and intensity of the 194 nm radiation, and its overlap with the ions, limit our typical stability to about twice that of Eq. (1).

The $^{199}Hg^+$ ground-state hyperfine structure further complicates laser cooling and state detection. For any constant laser polarization and zero magnetic field, two superpositions of the $^2S_{1/2}$, $F = 1$, $m_F = 0, \pm 1$ levels are dark states. After the ion optically pumps into these states, the fluorescence vanishes. To constantly pump the ions out of the dark states, the laser field must couple each $^2S_{1/2}$, $F = 1$, $m_F = 0, \pm 1$ level to the $^2P_{1/2}$, $F = 0$ level. Also, each of these three couplings must have a different time dependence. We satisfy these conditions with two non-collinear laser beams. One beam passes through a photo-elastic modulator whose calcite crystal axes are tilted ±45° relative to the beam polarization. The mechanical compression along one of the crystal axes is 90° out of phase with that of the other. The resulting changes in the crystal birefringence continuously cycle the laser beam's polarization state between left and right circular polarizations. The linear polarization of the second beam remains fixed in the plane formed by the two beams, which overlap with the ions at a 40° angle to each other.

Laser sources at 194 nm

The system currently used to generate 194 nm light [16] starts with radiation from a single-frequency argon-ion (Ar^+) laser at 515 nm. About 500 mW of this light is frequency-doubled in a cavity containing a BBO crystal to produce about 100 mW of 257 nm radiation. The remaining 5.5 W of Ar^+ laser light pumps a Ti:sapphire laser to make 500 mW of 792 nm radiation. The 792 nm and 257 nm beams are each enhanced in separate optical cavities, whose foci overlap in a second BBO crystal. This creates about 400 μW of 194 nm radiation through sum-frequency mixing. The repumping beam is made by overlapping a low-power diode laser with the Ti:sapphire beam before they both enter the power enhancement cavity. Beams from the Ti:sapphire and diode lasers are heterodyned, and the diode laser frequency is servoed to maintain the heterodyne signal frequency at 47.4 GHz.

The 40.5 GHz Microwave Clock

We use the Ramsey technique of separated oscillatory fields to probe the clock transition [17]. First, to cool the ions, both the primary and repumping 194 nm laser beams are pulsed on for 300 ms. Next, the repumping beam is turned off for about 90 ms, so that essentially all of the ions are optically pumped into the $^2S_{1/2}$, $F = 0$ level. Both beams are then blocked during the Ramsey microwave interrogation period, which consists of two

250 ms microwave pulses separated by the free precession period T_R, which we vary from 2 to 100 s. Finally, the primary beam is turned on for about 10 ms while we count the number of detected photons. This determines the ensemble average of the atomic state population, and completes one measurement cycle.

We synthesize the microwave frequency from a low-noise crystal quartz oscillator locked to a reference hydrogen maser [18]. To steer the average microwave frequency into resonance with the clock transition, we step the frequency by $+\Delta f$, then $-\Delta f$, about frequency f_M ($\equiv \omega_0/(2\pi)$), and complete a measurement cycle after each step. Usually, the stepped frequencies lie near the half-maximum points of the central Ramsey fringe. On successive measurement pairs, we alternate the signs of the frequency steps to avoid any bias due to a linear drift in, for example, the signal size. The difference between the number of detected photons for the pair of measurement cycles gives the error signal ε_M. A digital servo adjusts the average frequency according to

$$f_{M+1} = f_0 + g_p \varepsilon_M + g_i \sum_{m=1}^{M} \varepsilon_m , \qquad (2)$$

where f_0 is the initial value of the frequency, and the proportional gain g_p and the integral gain g_i are independent of each other. Typically, the maximum value of M for a single run is about 130. The average frequency for each run is calculated after discarding the first four recorded frequencies f_i, to negate initial frequency offsets.

Figure 3 shows the fractional frequency stability of the steered microwave frequency for seven ions and Ramsey times of 10 s and 100 s. When $N = 7$ and $T_R = 100$ s is $\sigma_y(\tau) \cong 3.3\ (2) \times 10^{-13}\ \tau^{-1/2}$, for $\tau \leq 2$ h. Consistently, $\sigma_y(\tau)$ is about twice the value expected from Eq. (1), primarily because of laser intensity fluctuations at the site of the ions. The measured frequency stability is comparable to those of the Cs beam standard NIST-7, for which $\sigma_y(\tau) \cong 8 \times 10^{-13}\ \tau^{-1/2}$ [19], and the Cs fountain standard, for which $\sigma_y(\tau) \cong 2 \times 10^{-13}\ \tau^{-1/2}$ [20].

Table 1 shows the most important corrections we make to the average frequency for

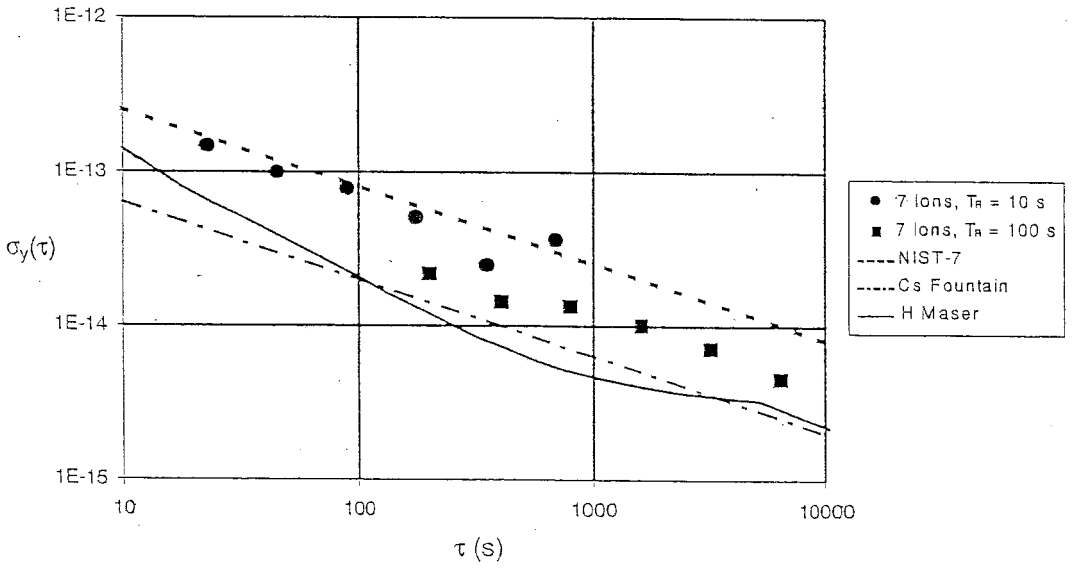

Figure 3: Stability plots for the 40.5 GHz microwave clock, using $N = 7$ ions, and both $T_R = 10$ s and $T_R = 100$ s. Also shown is the stability of the Cs beam standard NIST-7 [19], of the Cs fountain standard [20], and of the hydrogen maser.

each run [21]. The fractional Zeeman shift due to the static magnetic field is $+0.24\ B_{static}^2$, where B_{static} is expressed in teslas. The peak-to-peak variation in the static magnetic field between the beginning and end of a run is at most 1×10^{-8} T. Since the magnitude of the field is typically 3×10^{-7} T, an upper bound on the fractional uncertainty in this Zeeman shift is 1.4×10^{-15}.

We also correct for an ac Zeeman shift that depends linearly on the rf power P_{rf} delivered to the trap. The uncertainty in this correction dominates the overall uncertainty of the clock frequency. This shift can be caused by magnetic fields due to currents at frequency Ω in the trap electrodes that are asymmetric with respect to the trap nodal line. In an ideal trap, these asymmetric currents are absent. Allowing for this asymmetry to vary from load to load, we measure the average transition frequency for P_{rf} ranging from about 17 mW ($V_0 \cong 140$ V) to 68 mW ($V_0 \cong 270$ V) for each ion crystal. A fit to these data gives the frequency shift $(d\omega/dP_{rf})/\omega_0$ and the extrapolated frequency at zero rf power ω_0, for that crystal. Typically, $(d\omega/dP_{rf})/\omega_0 \cong (2.5 \pm 2.1) \times 10^{-16}$ /mW (within the uncertainty, this value is the same for each crystal), and the uncertainty in the extrapolated frequency averaged over five ion crystals used in the frequency measurement is 3.2×10^{-15}.

Frequency shifts due to the phase chirp of the microwaves as they are switched on and off (combined with a possible leakage microwave field present during the free precession time T_R), and to asymmetries in the microwave spectrum scale as $1/T_R$. By varying T_R, we measure the fractional shift from these combined effects to be -3 (3) $\times 10^{-14}$ /T_R (where T_R is in seconds). Finally, from the measured intensity of the scattered 194 nm light at the site of the ions when the 194 nm sources are blocked, the ac Stark shift due to stray 194 nm light present during the Ramsey interrogation time is $< 3 \times 10^{-16}$.

The fits to the transition frequencies as a function of rf power give the extrapolated

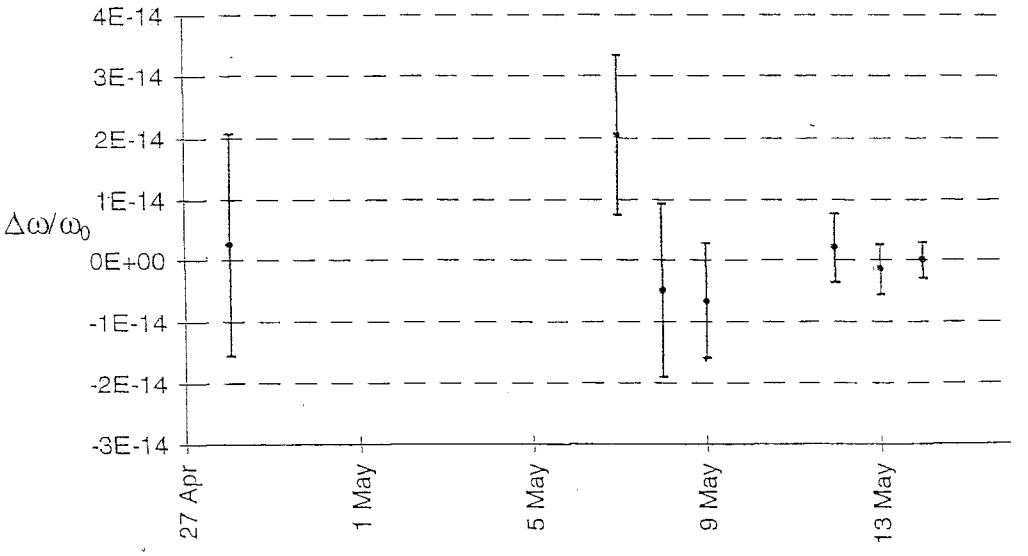

Figure 4: Summary of average frequencies over 18 days.

frequency ω_0 at zero rf power. Figure 4 shows the variation in ω_0 over 18 days, which include 42 runs made over seven days using five different crystals. The normalized χ^2 for these five frequency measurements is 0.77. If we assume that the frequency depends linearly on time, a fit to the data gives a drift of -5 (9) $\times 10^{-16}$/day, consistent with zero.

We compare the hydrogen maser frequency to the primary standards through International Atomic Time (TAI) [4] to obtain the average value

$\omega_0 = 2\pi \cdot 40\ 507\ 347\ 996.841\ 59\ (20)\ (41)$ Hz. The first uncertainty is due to the systematic shifts shown in Table 1 and is inflated to reflect the preliminary nature of this evaluation. The second uncertainty is due to the uncertainty in the frequency of TAI. The value of ω_0 may be compared with the previous most accurate measurement, which gave

Table 1: Systematic shifts of the average clock transition frequency. Typical values are for an rf power delivered to the trap of $P_{rf} = 20$ mW, a Ramsey interogation time of $T_R = 100$ s, and a static magnetic field of $B_{static} = 3 \times 10^{-7}$ T. Here, B_Ω is the magnetic field component at frequency Ω, I_p is the intensity of the scattered primary beam during the Ramsey interrogation time, δ_p the detuning of the frequency of the primary beam from that of transition p, and γ the linewidth of the cooling transitions.

Shift	Scaling	Magnitude of Effect (Typical)	Uncertainty in Effect
Quadratic Zeeman (static)	$+ < B_{static}^2 >$	2×10^{-14}	1.4×10^{-15}
Quadratic Zeeman (Ω)	$+ < B_\Omega^2 >$	5×10^{-15}	3.2×10^{-15}
Microwave chirp, leakage, and spectrum asymmetries	$1/T_R$	3×10^{-15}	8×10^{-16}
Light shift from 194 nm	$\frac{I_p \delta_p}{\delta_p^2 + \gamma^2}$	$< 3 \times 10^{-16}$	$< 3 \times 10^{-16}$

$\omega_0/2\pi = 40\ 507\ 347\ 996.9\ (3)$ Hz [22].

Future improvements to this standard include reducing the magnetic field at frequency Ω by decreasing Ω and the trap dimensions. Better magnetic shielding will reduce fluctuations in the static magnetic field, and use of a smaller, more tightly confining trap will allow linear crystals with more ions. By monitoring each ion individually, we can determine their internal states with negligible uncertainty, which will eliminate noise due to laser frequency and intensity fluctuations.

Optical Frequency Standard

We are now developing a frequency standard based on the $^{199}Hg^+$, 282 nm electric-quadrupole transition, which has a natural linewidth of 1.7 Hz. Since the clock transition frequency ω_0 is extremely large ($\omega_0/2\pi = 1.1 \times 10^{15}$), the fractional stability can be very high, as seen in Eq. (1). For example, for a single ion probed using the Ramsey technique with a free precession time of 30 ms (limited by the $D_{5/2}$-state lifetime), the fractional frequency stability is $1 \times 10^{-15}\ \tau^{-1/2}$

Previously at NIST, the frequency of a laser stabilized to about 30 Hz was doubled and then locked to this transition in a single ion confined near the Lamb-Dicke limit [23] in a room-temperature rf trap. Periodically, the laser frequency was scanned to obtain a laser-broadened linewidth of approximately 40 Hz at 563 nm [24]. However, the lifetime of the trapped ion was about ten minutes, as explained above. To thoroughly investigate such a frequency standard, long observation times are critical. We have built a second cryogenic system that will house a trap for this experiment, which should eliminate ion loss. We have constructed a linear trap such as that shown schematically in Figure 5. The rod electrodes are driven with an oscillating electrical potential while the "finger" electrodes are held at rf ground, which creates a pseudo-harmonic potential that confines the ions radially. The ions

are confined axially by properly adjusting the static potentials of the finger electrodes (see Fig. 5). The axial confinement in this trap can be much greater than that in the trap of Fig. 1, since the electric field from the "endcaps" is not shielded by the rf electrodes [7].

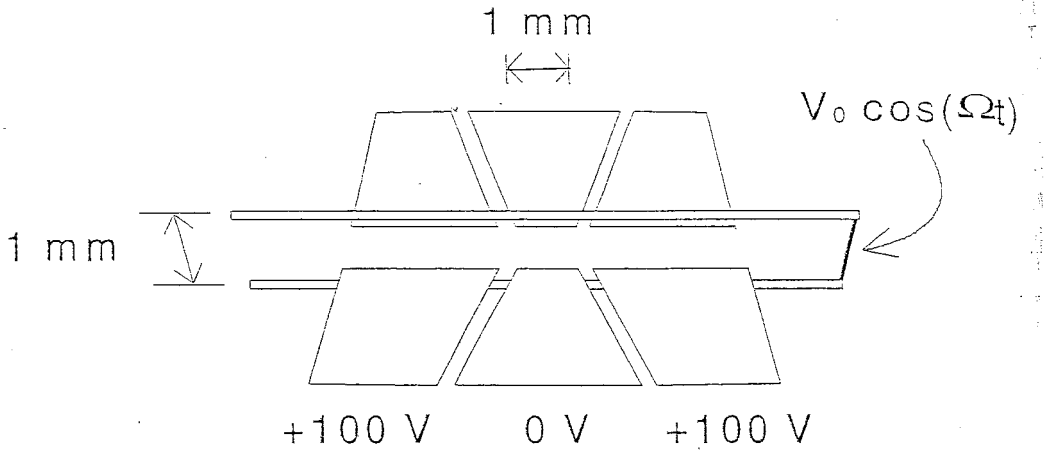

Figure 5: Tight-confining linear Paul trap.

Narrow-band laser source at 282 nm

To take advantage of the small width of the electric quadrupole transition, the 282 nm source driving the transition must have a linewidth comparable to or less than the transition width. The present system for generating 282 nm radiation consists of an argon ion laser pumping a dye laser that produces 500 mW of 563 nm radiation. The 563 nm light is frequency doubled by a single pass through a 90° phase-matched AD*P crystal to produce up to 100 μW of 282 nm radiation. When the 282 nm light is focused to about 25 μm and there is no broadening, less than 1 pW will saturate the quadrupole transition.

The frequency of the 563 nm laser is stabilized in two stages [24]. First, the dye laser frequency is stabilized to a cavity with a finesse of about 800 using the Pound-Drever-Hall technique [25]. Low-frequency fluctuations are removed with an intracavity piezo-mounted mirror, while the high-frequency fluctuations are removed by a fast (servo bandwidth > 2 MHz) intracavity electro-optic modulator. When the servo loops are closed, the laser linewidth is reduced to about 1 kHz. Then the stabilized light is transmitted through separate optical fibers to high-finesse cavities. Again, the Pound-Drever-Hall technique is used to lock the frequency of the fiber-transmitted light to the cavity frequency. Long-term corrections to the laser frequency, determined by one of the high-finesse cavities, are fed back to the length of the lower-finesse cavity. Higher-frequency fluctuations are removed with an acousto-optic modulator. The frequency-stabilized light from either cavity is directed towards the trapped ion.

The high-finesse cavities have been described elsewhere [24]. The spacer of one of the two cavities is made of a 27 cm long, 10 cm diameter Zerodur rod, and that of the second cavity is made of a 10 cm long, 10 cm diameter ULE rod. Both spacers have a hole bored down the rod axis to transmit light. The transmitted power, and hence the intracavity power, are stabilized to 0.1%. High-reflectance mirrors, whose radii of curvature are chosen so that the modes of the cavities are highly non-degenerate, are optically contacted to the ends of each rod. Each cavity is suspended by two thin tungsten wires inside separate vacuum chambers, whose temperatures are actively stabilized. Each cavity, much of the optics and some of the electronics are mounted on separate platforms, which are suspended by several

sets of rubber surgical tubing to isolate the cavities from floor and ceiling vibrations. The tilt of each suspended platform is stabilized by servoing the distance of three of its corners from the floor by heating the rubber tubing to adjust its length. The cavity and platform are enclosed in a particle-board box lined with thin layers of lead and foam to reduce acoustical vibrations.

Figure 6 shows a beat note between two laser beams locked to these two independent

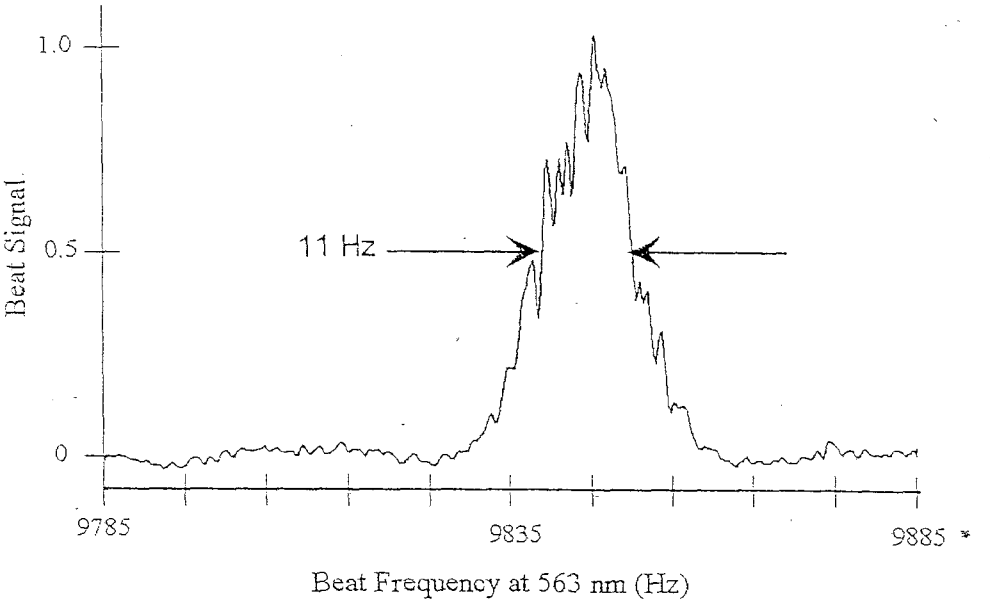

Figure 6: Beat note between two laser beams locked to independent cavities, integrated over 80 s. The full width at half-maximum is 11 Hz.

cavities. The full width at half-maximum is approximately 11 Hz. If both lasers have the same linewidth, the linewidth of a single laser is about 8 Hz. This is fractionally 1.5 parts in 10^{14} of the laser frequency at 563 nm, which we think is the narrowest recorded linewidth.

All Solid-state Laser Systems

To make the 194 nm and 282 nm radiation sources more compact, reliable and stable, we are converting them to an entirely solid-state design. The Ti:sapphire laser can be replaced by an injection-locked diode laser that produces over 500 mW of 792 nm radiation [16, 26]. The Ar^+ laser will be replaced by a 1 W single-frequency, diode-pumped, frequency-doubled Yb:YAG laser at 1.029 μm [27]. Since the doubling efficiency in 90° phase-matched $KNbO_3$ or LBO can be 50% [28], we expect to generate over 500 mW of 515 nm radiation. This will be doubled as before, then summed with the radiation at 792 nm to generate more than 100 μW of light at 194 nm.

To convert the 563 nm source to a solid-state system, the dye laser and pump laser will be replaced by a diode-pumped Nd:FAP laser at 1.126 μm. Approximately 100 mW of single-frequency radiation from the Nd:FAP laser has been frequency-doubled in angle-tuned $KNbO_3$ to produce 7 mW of 563 nm radiation. The light at 563 nm can be frequency-doubled as before to generate about 2 μW of 282 nm radiation.

Summary

We have locked a synthesizer to the 40.5 GHz transition in laser-cooled crystalline strings of $^{199}Hg^{+}$ ions in a linear cryogenic rf trap. With a Ramsey period of 100 s and seven ions, the fractional stability of the microwave frequency is $3.2 \times 10^{-13} \cdot \tau^{-1/2}$ for measurement times $\tau < 2$ h. We have measured the clock transition frequency with a fractional statistical and systematic uncertainty of about 5×10^{-15}. This uncertainty is primarily limited by the uncertainty in the Zeeman shift due to fields at the trap frequency Ω and can be reduced in several ways. We are developing a cryogenic 282 nm optical frequency standard, whose potential stability is $\sigma_y(\tau) \approx 10^{-15} \tau^{-1/2}$. The lasers used to drive the 282 nm electric dipole transition have a frequency stability of less than 10 Hz for times from 1 to 80 s. Finally, we are converting our laser systems to entirely solid-state designs, which should allow longer continuous running times for both the microwave and optical frequency standard.

This work was supported by ONR and ARO. We thank Don Sullivan, Elza Vasconcellos, Steve Waltman and Matt Young for carefully reading this manuscript.

References

* Work of US Government; not subject to US copyright.

1 R.C. Thompson, in Adv. At. Mol. Phys. **31**, 63 (1993), and references therein.

2 J.J. Bollinger, W.M. Itano, D.J. Wineland, and D.J. Heinzen, Phys. Rev. A **54**, R4649 (1996).

3 Proc. 5th Symp. Freq. Standards and Metrology, ed. J.C. Bergquist (World Scientific, 1996).

4 Proc. IEEE: Special Issue on Time and Freq. **79** (7), (1991).

5 R.L. Tjoelker, J.D. Prestage, and L. Maleki, in Ref. 1, p. 33.

6 P.T.H. Fisk, M.J. Sellars, M.A. Lawn, and C. Coles, in Ref. 1, p. 27.

7 M.E. Poitzsch, J.C. Bergquist, W.M. Itano, and D. J. Wineland, Rev. Sci. Instrum. **67**, 129 (1996).

8 H.G. Dehmelt, in Frequency Standards and Metrology, ed. A. DeMarchi (Springer, Berlin, 1989), p. 286.

9 J.D. Prestage, G.J. Dick, and L. Maleki, J. Appl. Phys. **66**, 1013 (1989).

10 D.J. Wineland, Wayne M. Itano, J.C. Bergquist, J.J. Bollinger, F. Diedrich, and S.L. Gilbert, Proc. 4th Symposium on Freq. Standards and Metrology, ed. A. Demarchi (Springer Verlag, Heidelberg, 1988).

11 W.M. Itano, J.C. Bergquist, J.J. Bollinger, J.M. Gilligan, D.J. Heinzen, F.L. Moore, M.G. Raizen, and D.J. Wineland, Phys. Rev. A **47**, 3554 (1993).

12 D.J. Berkeland, J.D. Miller, J.C. Bergquist, W.M. Itano, and D.J. Wineland (submitted for publication in Phys. Rev. A, August, 1997).

13 M.G. Raizen, J.M. Gilligan, J.C. Bergquist, W.M. Itano, and D.J. Wineland, Phys. Rev. A **45**, 6493 (1992).

14 W.M. Itano, L.L. Lewis, and D.J. Wineland, Phys. Rev. A **25**, 1233 (1982).

15 W.M. Itano, J.C. Bergquist, J.J. Bollinger, J.M. Gilligan, D.J. Heinzen, F.L. Moore, M.G. Raizen, and D.J. Wineland, Phys. Rev. A **47**, 3554 (1993).

16 D.J. Berkeland, F.C. Cruz and J.C. Bergquist, Appl. Opt. **2006**, 4159 (1997).

17 N.F. Ramsey, *Molecular Beams* (Oxford Univ. Press, London, 1956).

18 C.W. Nelson, F.L. Walls, F.G. Ascarrunz, and P.A. Pond, Proc. 1992 IEEE Freq. Control Symp., 64 (1992).

19 W.D. Lee, J.H. Shirley, J.P. Lowe, and R.E. Drullinger, IEEE Trans. Instrum. Meas. **44**, 120 (1995).

20 A. Clairon, S. Ghezali, G. Santarelli, Ph. Laurent, S.N. Lea, M. Bahoura, E. Simon, S. Weyers, and K. Szymaniec, in Ref. 1, p. 27.

21 D.J. Berkeland, J.D. Miller, J.C. Bergquist, W.M. Itano, and D.J. Wineland (submitted for publication in Phys. Rev. Lett., October, 1997).

22 L.S. Cutler, R.P. Giffard, and M.D. McGuire, Proc. 13th Ann. PTTI Appl. And Planning Meeting, NASA Conf. Publ. 2220, 563 (1981).

23 R.H. Dicke, Phys. Rev. 89, 472 (1953).

24 J.C. Bergquist, W.M. Itano, and D.J. Wineland, Frontiers in Laser Spectroscopy, 357 (1994).

25 R.W. P. Drever, J.L. Hall, F.V. Kowalski, J. Hough, G.M. Ford, A.J. Munley, and H. Ward, Appl. Phys. B **31**, 97 (1983).

26 F.C. Cruz, M. Rauner, J.H. Marquardt, L. Hollberg, and J.C. Bergquist, in Ref. 1, p. 511.

27 P. Lacovara, H.K. Choi, C.A. Wang, R.L. Aggarwal, and T.Y. Fan, Opt. Lett. **16**, 1089 (1991).

28 Z.Y. Ou, S.F. Pereira, E.S. Polzik, and H.J. Kimble, Opt. Lett. **17**, 640 (1992).